XRD Studies on Metamorphic Changes of the Dissimilarly Graphitized Carbonaceous Materials

ABSTRACT: One of the unique yet functional properties of the carbonaceous materials is an irregular change in their internal heterogeneity and graphene layouts upon graphitizing themselves. The precise investigations of such type phase transitions inclusive of reshuffling/restructuring of the sporadically arranged graphene C–atoms, and thereby acquiring crystallite growths & contractions, crystallinity, graphitization degree, extent of structural orders, dissimilar range pores & porosity networks, etc., are indispensable for understanding the actual transformation aptitudes of the low temperature amorphous carbons into the crystalline semi-graphite and graphite like functional materials. In this report, the XRD spectroscopy is applied to the variably carbonized and graphitized carbon materials (activated carbons (AC1─AC3) & carbon blacks (CB1─CB4)), and the progressive internal improvisations in their graphene layouts caused by the dissimilar metamorphic temperature regimes are sought out. For this, the XRD diffractograms linked descriptors (diffraction angles (2θ), intergraphene layer gap (d), & crystallite sizes (L_c)), and the correlations between many descriptive subordinates (% crystallinity (%C), graphitization degree (%DOG), metamorphic temperature (T_{met}), BET surface area (S_{BET}), and specific capacitance (C_{SP})) are taken into account. The former set speculates the existence of lower amorphicity and higher graphitic homogeneity in CBs than in the ACs, and elucidates their contrasting inbound graphene configurations. And, the latter set quantifies the extent to which the founding graphitic units of them undergo significant improvements owing to acquire better functional domains. The applicative propensities for them are forecasted as CB4 (C = 1.3%, DOG = 98%, T_{met} = 595°C, S_{BET} = 5348 m^2/g, C_{SP} = 600 F/g) > CB3 (C = 5.1%, DOG = 96%, T_{met} = 588°C, S_{BET} = 3735 m^2/g, C_{SP} = 419 F/g) > CB2 (C = 5.8%, DOG = 93%, T_{met} = 576°C, S_{BET} =1508 m^2/g, C_{SP} = 169 F/g) > CB1 (C = 19.7%, DOG = 64%, T_{met} = 486°C, S_{BET} = 1186 m^2/g, C_{SP} = 133 F/g). The author believes these datasets as quite useful while specifying their compressibility & reinforcement, binding & lubricity, catalysts & catalysis, electrochemical & electro-adsorption, etc., and can be referred time to time while identifying distinctive functionalities of one over the others.

KEYWORDS: Carbon Blacks, Graphitization, Metamorphisms, BET Adsorption, Capacitance

1. INTRODUCTION

In the material science domain, carbon is second only to cement in its widespread use due to its functional properties. The naturally available graphite and diamond are two of its most abundant ultra-useable materials wherein the founding elemental carbon networks are arranged with SP^2 (hexagonal lattice) and SP^3 (tetrahedral) hybridization geometrical patterns respectively bestowing relatively higher degree of internal crystallinity. Few other allotropic forms of it possessing many contrasting yet promising characteristic features of the nanomaterials, and do have high degree of crystallinity, but are derived synthetically whose internal structural arrangements are verified by the first principle theoretical/computational calculations are fullerene (buckyball) [1], cylindrical fullerene (fullertube) [2], metallic 3D cage structured carbon (Q-carbon) [3], etc. And, some carbonaceous forms of it that are highly amorphous with no long range crystalline orders (low degree of crystallinity), no any predetermined geometrical shapes gained by the repeatedly arranged C atoms, and have sporadical atomic arrangements, localized π-electron systems with dangling type C─C π-bonds are activated carbons, carbon cokes, glassy carbons, charcoals, carbon blacks, carbon stars, etc. [4]. In the thermochemical processes of converting natural carbon-enriched organic materials into many of those synthetic carbonaceous materials, oxidative and non-oxidative carbonization techniques are very frequently preferred where the precursor carbon materials are excessively burnt under complete absence of oxygen at variable temperature regimes, and the gaseous traces such as CO_2, CH_4, H_2S, COS, H_2O, etc., are eliminated completely from the variable functional groups held into them. And, in the thermodynamical heat treatment processes of increasing internal degree of crystallinity in thus produced amorphous and low-crystalline ordered carbonaceous materials, graphitization technique is widely used by means of which the carbon atoms within the internal networks undergo structural rearrangement, and the atomic layouts and periodicities are improved with the betterment in the internal orders of the

graphene layers. Nevertheless, the common strategical goals of both of these heat treatment techniques are to fabricate the exceptionally large surface-area graphitized carbon materials, and to convert & modify low graphitic type carbon materials into the more graphitic with the exceptional introductions of the hierarchical pores along with improvising various applicative morphological, thermal, mechanical, electrical, and electronic properties such as internal degree of porosity and porous networks; specific surface area; irregular shapes (cylindrical, inkpot, tubular, etc.) and sizes of the porous structures (macro– (> 50 nm), meso– (2–50 nm), and micro–pores (< 2nm)); heterogeneous textures of the interior and exterior grainy matrices; electrical-energy-storing, conductive, and self-healing propensities; lightweight, more stiffness, thermal expansion resisting, and chemical stability retaining features; etc. [5–10]. However, the graphitization technique is particularly taken as more rigorous heat treatment procedures of making the internal layouts of the graphitic layers of the carbonaceous materials more and more ordered with the effective improvisations on degree of crystallinity, heat and thermal conductivity rates, ionic and electrical energy storing potentialities, friction and lubrication attributes, oxidative resistivity, etc., and the recognizable lowering of the coefficient of frictions, materials hardness & strength, etc. In other words, graphitization simply refers to restructuring of the internal arrangements of the graphitic layers of the low crystalline and amorphous type carbonaceous materials through the uses of wide range metamorphic temperature (T) regimes, and to converting either of them into the graphite resembling materials so that all those specific physicochemical properties offered by them become fully functionalized practically. In particular, this temperature dependable changings of the internal layouts of the carbon networks that induce them to gain all those improvised properties are furthermore clarified as; at (a) T = 30–1300^{o}C (hard carbon materials), the very minimal internal changes begin to take place in the carbon layouts of substrate

amorphous carbonaceous materials such as slight rearrangements of smaller graphene domains (basic structural units (BSU)), breaking down of the more disordered C–C bonds, and complete removal of the volatile organic traces, etc., (b) T = 1300–2000°C (moderately soft carbon materials), the significant atomic movements and internal rearrangements of the graphene C–atoms, and their considerable restructurings (more and more breakage of the in-built amorphous C–C links, rapid formation of the new type C–C bonding linkages between the planes and intertwined areas, and fine conversion of more chaotic orders of graphene layers into the more systematic) take place with the remarkable shrinkage on the intergraphitic layer spacings (d), and (c) T = 2000–3000°C (soft carbon materials), the perfect crystal growth occurs with the optimum ordering of the graphene layers (all the chaotic orders attain standard alignments and locations almost ideal to the graphite), maximum reduction in the d value, highest increment in the degree of crystallinity, crystallite sizes and growths, and the finest approaching of the resulting materials towards smooth-, homogeneous-, reproducible-, ordered-, and linearly aligned- graphene layers packing graphite [5, 7, 11, 12]. In fact, the same high temperature graphitized graphite like grainy materials are known for the basic founding constituent materials of the presently existed carbon made commercial products prevailing across the industrial sectors worldwide.

Few more predominating functionalisable attributes that lead the wide range carbonaceous materials in the paths of righteousness and promising industrial inventions are exceptional electrical, optical, thermal, conductive, catalytic, mechanical, chemical, and stabilization properties; large surface area to volume ratio; highly porous and internal porosity networks; good adsorbent and adsorbing propensities; relatively non-toxic, recyclable while employing in ultrafine filtration technologies; fundamental basis of fabricating 0D–3D type nanomaterials; etc. The most preferential selection of them in ultra -filtration, -purification, and -osmosis technology; carbon

capture and storage (CCS); controlling organic, inorganic, and biological pollutants; energy storage- batteries, solar panels, capacitors, supercapacitors, and many other high-tech devices, automotive industrial spare parts such as brake linings, mechanical seals, engine parts, etc.; military and commercial planes, sporting goods, and construction favorable materials, etc. [3, 5, 9 –13] further strengthen their global courtesy. In principle, greater the degree of graphitization, more improvised are the physicochemical properties, and better are the performances and functionalizing essences of the resulting carbon matrices. And, the very intensive internal improvisations that vow to offer all those physicochemical properties are (a) higher Young's modulus cum lower compressibility, (b) greater electrical and thermal conductivity, (c) better chemical, heat, pressure, etc., resistive stability, (d) more chemical oxidation withstanding ability, (e) substantial decrement in chemical reactivity, etc. [14]. Despite saying this, the carbon materials approaching more towards the graphitic structures are found to suffer from the larger volume expansions and lower electrochemical/electrode reactions kinetics, and more electrochemical imbalances between the adsorption and intercalation mechanisms of the electroactive ionic specimens [14–16]. Towards these, the relatively less soft type carbonaceous materials are marked to perform better in ions and energy storage capacity, low operating potential, more balanced ionic adsorption and intercalation mechanisms, relatively less reduced volume expansion, and many other promising electrochemical functions. Instead, the hard carbons characterized with very heterogeneous-porous matrices are remarkably noted to exhibit low initial coulombic efficiency, tap tendency, and volumetric electrode capacity even though they equally show the reduced volume expansion, comparable ion storage capacities, higher electronic conductivities, low cost processabilities, etc. [15, 16].

Owing to all those electrochemical, morphological, mechanical, etc. factors governed apparently distinctive physicochemical properties of the soft-to-hard range carbonaceous materials, many types of them are functionalized practically as potential electrode materials for different type battery technologies, fuel-cells, and capacitors & supercapacitors; solar cell films and endurable coatings; ultrasensitive sensor designations, and many other modified yet conductive electrode materials. The same are the triggering factors for conducting this research work wherein the various type carbonaceous materials (activated carbons (ACs) and carbon blacks (CBs)) manufactured industrially with wide range graphitizing temperature regimes (T = 800°C ─ 2500°C) are sampled, and characterized by X-ray diffraction (hereafter, XRD) spectroscopic technique. The closely associated spectroscopic parameters such as 2θ angular position, width and intensity of the bands, degree of their diffuseness/sharpness, integral area under them, etc. are fully assessed while revealing their grain morphologies, granular complexities, graphitic orders and graphene layers alignments, crystallinity, degree of approaches towards the standard graphite upon the increment of metamorphic temperatures, structural disorders, adsorbing capacities, porous and porosity textures, and amount of charge stored per unit mass of them. The responsible subordinates descriptive and deterministic to all those characteristic traits are Scherrer's formula based crystallite sizes L_c, Bragg's law derived interlayer distance d (basal spacing), Franklin's relation computed structural disorder (ρ) and degree of structural order (u), Seehra and Pavlovic (lately modified by Ivashita *et al*. [17]) formula estimated degree of graphitization (%*DOG*), Vlahov and Wada *et al*. proposed formula predicted metamorphic temperature ($T_{met.}$ (^{0}C)), full-width at half maximum (*FWHM*) of the XRD-band interlinked degree of crystallinity (%*C*), *Lc* and X-ray density (ρ_{xrd}) dependent BET surface area (S_{BET}), and electrical double layer capacitance (C_{dl}) & S_{BET} dependent specific capacitance (*Csp*). The entire article is structured herewith as: Materials

& Methods in section 2, Results & Discussions in section 3, and Summary & Conclusions in section 4.

2. MATERIALS AND METHODS

2.1 Collection of the Selected Carbonaceous materials

The low, moderate, and high graphitizing temperature (*T*) regimes treated carbonaceous materials (activated carbons, and carbon blacks) were directly procured from the designated industries (mostly from Toray Industries, Inc.) that manufacture them in large scales, and supply the same worldwide as ideal electroactive carbon materials. The explicit selections and declarations of them as the most potential experimental specimens for the present research work were meticulously done by considering their promising type physicochemical properties and the overall functionalizing possibilities practically towards the progressive advancements and innovations of the futuristic electroactive materials needful for designing new generation battery technologies, capacitors, supercapacitors, and ultrasensitive biosensors. Based on their graphitizing temperature regimes disclosed by the specific manufacturers and the effective guidelines they follow for the entire manufacturing processes, the carbon samples taken herewith as experimental specimens were categorized as: (a) T = ~600–900°C; Activated carbons (AC1, AC2, and AC3), (b) T = ~800°C; carbon black (CB1), (c) T = ~1400°C; carbon black (CB2), (d) T = ~2000°C; carbon black (CB3), (e) T > 2500°C; carbon black (CB4). These samples were named randomly without any prior orders of their manufacturers just to maintain their confidentialities including specific industries, commercialized brand names, industrially revealed R & D characteristic features, service catalog properties, and the overall copyright policies & memoranda. While delivering each of them for the explicit XRD measurements, the required amount of them was kept separately into the moderately hard type polyethylene bottles labelled priory with the designated symbols, and

each one of them was made perfectly air-tight, and moisture-sealed with aluminum foil layered stoppers. The ultrafine grainy particulates were securely protected from the humid weather exposures, accidental spilling and breakages, and their entire morphological & external textures along with preserving the consistencies of their particulate surfaces correlated characteristic physicochemical properties.

2.2 Measurements of the XRD Diffractograms

Since the specific collaborating wing where the author was affiliated with was not equipped with the X-Ray diffraction facility needful to this instrumental characterizations based experimental study, all the carbon sample holders (air-tight polyethylene made hard bottles) were delivered to the designated "Integrated Industry-Academia Facility; an industrially funded research hub center established mainly to advance the industrial R & D activities. As per its daily operational guidelines, and R & D advancement integral policies, the XRD facility was made accessible directly to the both academic and industrial institutions, and the prompt technical supports such as (a) instrumental handling, (b) XRD measurements, (c) in-built software based databases fitting techniques, etc., type services were provided as per the requirements of the customers. The XRD instrument available therewith, and was operated for the present measurements of Activated Carbon (AC1, AC2, AC3, AC4), and Carbon Black (CB1, CB2, CB3, CB4) was bench-top diffractometer BRUKER D2 PHASER (characteristic with florescence under Copper X–rays). The XRD diffractograms for every carbon sample specimens were obtained in an 2θ angular regime of 10–90°, an angular increment step size of 0.02°, and a material scanning rate of 0.5°/min. All the internal calibrations and standardizations of the XRD machine with first order diffraction were set as per the operational manual prescribed by the manufacturer.

2.3 Determinations of the XRD Spectral Descriptors

In the course of analyzing the XRD spectral patterns of each carbon black sample (CB1, CB2, CB3, CB4), the most intense XRD band arose at the specific diffraction angle (2θ) was firstly identified, and retrieved the required datasets (intensity vs 2θ) explicitly followed by their subsequent subjections to the *Gaussian* convolutions for peak fitting. Being the activated carbon samples AC1, AC2, and AC3 low temperature heated carbonaceous materials (600─900^{o}C), the spectral bands and their peak heights were observed as incomparable to that of the carbon blacks (CBs). Therefore, the concerned spectral peak fittings were skipped herewith. While plotting the standard *Gaussian* convolutions in a three dimensional space, the specific Cartesian coordinates were programmatically created, and the required modifications were carried out as per the needs of the present live-simulation peak fitting procedures conducted in the Microsoft Excel spreadsheet. The controlling parameters such as peak height (H), peak width (W), and full-width at half maximum (herewith, FWHM (β)) were determined explicitly for every individual samples. The specific 2θ angle recorded for the same most intense XRD peak (fitted with the *Gaussian*) of each carbon black sample was used as a numeral value while finding out its intergraphene layer distance d_{CB} through Bragg's law of diffraction formulated in Eq. 1.

$$n\lambda = 2d_{CB}\, sin(\theta) \quad (1)$$

Where;

n = order of diffraction (by convention, the first order (n =1) diffraction was set for the XRD).

λ = wavelength of the incident X–ray ($\lambda = 1.54$ Å (*Cu Kα* wavelength))

θ = angle of incidence($\theta = 2\theta/2$)

And, the FWHM (β) (*rad.*) value computed for each carbon sample was used to estimate the specific crystallite size L_c *via* the Scherrer's mathematical relation formulated in Eq. 2

$$L_c = \frac{K \times \lambda}{\beta \times cos\theta} \quad (2)$$

Where;

K = Scherrer's constant.

The numeral value for the constant K was approximated using the relation shown in Eq. 3; an especially recommended formula for those cases where the (a) FWHM is determined through *Gaussian* peak fitting technique alike to this work, and (b) material specimen is comprising with the spherical or quasi-spherical type particulates (all the grainy carbon blacks are agglomerated form of the quasi-spherical type premiere particulates) [18]).

$$K = 2\sqrt{(\ln 2)/\pi} \cong 0.9394 \text{ [19]} \quad (3)$$

Each specific value of the L_c and d_{CB} determined for the CB1, CB2, CB3, and CB4 samples were directly substituted in Eq. 4, and the respective number of their parallel interatomic graphitic planes (m) stacked one over the other periodically or sporadically were determined.

$$m = \frac{L_c}{d_{CB}} \quad (4)$$

2.4 Formulations of the XRD Linked Subordinates

While the real-time simulations (*Gaussian* convolution fittings) of the most intense XRD spectral bands projected on the 2θ value: CB1: 2θ = 19.48°; CB2: 2θ = 24.66°; CB3: 2θ = 25.54°; and CB4: 2θ = 26.04° were on the fly, the net Area ($A_{carbon\ black\ peak}$) under every precisely-fitted spectral band was estimated separately *via* the relation expressed in Eq. 5; a standard formula recommended for approximating the net area under the typical *Gaussian* peak [20]. Thus calculated $A_{carbon\ black\ peak}$ (mm^2) values for every carbon black samples were substituted in Eq. 6 [17], and the percentage crystallinity ($\%C$) for each of them was speculated.

$$A_{carbon\ black\ peak} = \frac{\beta \times H}{0.3989 \times 2.35} \quad (5)$$

$$Crystallinity\ (C) = \frac{A_{graphite\ peak}}{A_{graphite\ peak} + A_{carbon\ black\ peak}} \times 100\ \% \quad (6)$$

Where;

$A_{graphite\ peak}$ = 200 mm^2; a standard area under the typical graphite (XRD) peak (2θ = 26.70^o [8, 17].

Similarly, the degree of graphitization (%DOG) for each carbon black sample was computed using the relation shown in Eq. 7; a standard formula proposed firstly by Seehra and Pavlovic, and modified lately by Ivashita *et al*. [17].

$$DOG\ (\%) = \left[1 - \left\{\frac{d_{CB} - d_g}{d_g}\right\}\right] \times 100\ \% \quad (7)$$

Where;

d_{CB} = intergraphene layer distance of the carbon black (Eq.1),

d_g= intergraphene layer distance of the typical graphite ($0.33354\ nm$) [8, 17].

Again, the Vlahov and Wada *et al*. derived mathematical formula (Eq. 8) [17] was employed to predict the metamorphic temperature ($T_{met}(^0C)$) gained by each carbon black sample; a gradual internal kinetic energy increasing temperature affecting the internal shifting of the atomic positions (vibration of the atoms) of the graphitic layers within the definite crystal lattice consecutively [21].

$$T_{met} = (3.2 \times DOG(\%) + 280) \quad (8)$$

And, the Franklin's relations (Eq. 9a and 9b) were used to estimate the internal structural disorder (ρ) and degree of structural order (u) respectively; the potential parameters deterministic to reveal an internal heterogeneity or the core-level layouts of the graphene planes of the carbon materials.

$$\rho = \sqrt{\left[1 - \left(\frac{3.440 - d_{CB}}{0.086}\right)\right]} \quad (9a)$$

$$u = 1 - \rho \quad (9b)$$

Accordingly, the net BET adsorption surface area ($S_{BET} \approx S_{XRD}$ (m^2/g) offered by every carbon black samples was approximated by the relation given in Eq. 10; a physical structure (surface

irregularities and porous networks/walls) and an internal/external morphology forecasting indicator explaining how actually the carbonaceous materials interact with the particular environment.

$$S_{BET} = \frac{2}{\rho_{xrd} \times L_c} \times 1000 \quad (10)$$

Where;

$\rho_{xrd} = \frac{d_g}{d_{CB}} \times \rho_{graphite}$, (an X-ray density of carbon) (11)

$\rho_{graphite} = 2.265 \pm 0.001$ (g/cm^3), an X-ray density measured for the ultrapure graphite [22]. Lastly, the mathematical relation shown in Eq. 12 was used to determine the specific capacitance C_{SP} (F/g) of all the four carbon black samples; the electrochemical descriptor illuminating the net amount of charge stored per unit mass of them while employing as electrode materials for batteries, capacitors, and supercapacitors.

$$C_{SP} = \left[C_{dl} \times \frac{S_{BET}}{2}\right] \times 10000 \quad (12)$$

Where;

$C_{dl} = 2.244 \times 10^{-5}$ (F/cm^2); a typical literature value [9, 23] of the electrical double layer capacitance of the electrochemical double layers constructed in the electrode-electrolyte interfaces.

3. RESULTS AND DISCUSSIONS

3.1 Validations of the XRD Spectroscopy

The rational applications of the XRD spectroscopic methods in characterizing the wide range materials both by qualitative and quantitative scales are not new in material science domains [24, 25]. More importantly, the ultrafine grainy and non-grainy matrices comprising with the distinguished crystallite phases and sizes in the core granular level, which in fact not only acts as a fingerprint basis of their explicit characterizations but also significant means of finding out their

founding phases; agglomeration propensities of their crystallites, grains, and particulates; packing tendencies and coefficients owing to gain definite crystalline shapes and geometries, materials compressive strength, etc., are imperative type materials for the genuine specifications and in-built characterizing functions of the XRD machine [6, 8,15]. The Bragg's law of diffraction (Eq. 1) is the major mathematical formulation by means of which the entire working principles of the XRD and the relevant theoretical interpretations are carried out: the 2θ angular values in which the specific XRD bands are protruded are directly correlated to the periodically repeated interatomic layers gap (d), and themselves are the primary parameters for identifying founding crystallite phases of the materials. The carbonaceous materials derived through the direct or the chemical processes-induced carbonizations of the naturally available carbon precursors, and are improvised with the recognizable physicochemical properties successively through the metamorphic heat treatments under variable graphitizing temperature regimes belong to the same type XRD ultrasensitive material. Like many other applicative material domains, they hold the crystallite phases but of the least or less or more ordered graphene domains (basic structural units (BSU)) packed each other through Van der Waals force of interactions, and do exhibit the substantial change in sporadical arrangement of the BSU, degree of crystallinity (%C), internal heterogeneity, core-level layouts of the graphene planes, etc., upon the variations of the metamorphic temperature scales ($T_{met.}$). Additionally, few of the $T_{met.}$ (^{o}C) dependent contrasting yet functional characteristic features of them owing to perform differently as hard, moderate, and soft type carbonaceous materials such as variable crystallite sizes (L_c) and their conglomeration tendencies, unequal number of the parallel graphene layers arranged with the gap d, dissimilar internal packing ratios of the graphitic planes leading to attain irregular, distorted, and/or regular crystal geometries, inequivalent internal rearrangement of the graphitic layouts, dissimilar atomic vibrations and

restructurings of the founding dangling C─ C bonds, etc., demand high performance ultra-surface sensitive powder XRD technique for the precise scanning of them instrumentally. Besides these, the XRD spectroscopy cum diffractograms retrieved databases are directly applicable towards predicting the grain sizes and compressive strengths, surface textures and exterior/interior morphologies of the particulates, porosity and microstructures, high or low adsorbing trends with size selectivity (BET surface area), better or weaker ultra-filtering potentialities, good or bad electroactive specimens (ions/molecules) storing capacities, chemical affinities of the binding materials and moistures, and many other electrochemical attributes such as rapid or sluggish ionic intercalations, more or less balanced ionic adsorption and intercalation mechanisms, relatively less or more reduction in volume expansions, etc. Herewith, the wide range hard and a relatively soft carbonaceous materials treated industrially with the dissimilar range graphitizing temperatures (*T*): (a) T = 600°C─900°C; activated carbons (AC1─AC3) and (b) T = ~800°C─ > 2500°C; carbon blacks (CB1─CB4) are practically considered as the most appropriate experimental specimens, and the powder XRD spectroscopic method was employed to scan all their grainy particulates instrumentally. Thereafter produced XRD spectral datasets, and the crystallite phases diffractions based standard variables are incorporated to speculate many of their morphological and electrochemical macroscopic and microscopic physicochemical observables.

3.2 Interpretations of the XRD Diffractograms

Since the "Activated Carbon (AC1, AC2, AC3)" samples are industrially produced simply by burning the wide range carbon precursor materials, and are not treated at all with any ranges of the graphitizing temperatures (> 1000°C), all the required XRD interpretations are begun herewith from their respective diffractograms displayed in Figure (1). While doing so, more quantitative clarifications regarded to the significant variations in the internal rearrangements/restructurings of

the graphitic basic structural domains, altering of the internal degrees of the crystallinity (%*C*), changing of the crystallite sizes and conglomeration tendencies, etc., upon changing metamorphic heat treatments can only be presented logically. Absence of the sharp spectral bands in the Figure (1) indicates that none of the AC samples possesses significantly ordered structural repetitions of the graphene layers. The sporadical layouts or the heterogeneous structures of the fundamental graphitic domains arranged internally as basic building blocks of such type amorphous carbonaceous materials actually causes the intensive peak broadening effects and therefore, led the band protruded with highly diffused bump at 2θ = 44.5°, but null at 2θ = 25^0—27^0. The first diffraction angle is a characteristic value descriptive to the high degree of amorphicity whereas the second one is deterministic to the existence of low to high range graphitic orders and graphite like crystallites [26]. The somewhat negligible protrusions appeared in the latter 2θ range elucidate that the pronouncedly existed internal amorphicity of all the three activated carbon samples can be improvised gradually, and transformed into the recognizable crystallinity subsequently upon the increment of the graphitizing temperature scales. It further guaranties that all these amorphous or low temperature carbonized materials can be graphitized (the potential precursor materials for the intensive graphitizations), and transformed into the more applicative carbon domains successively. Despite observing relatively broad type bumpings at the former 2θ value, the present author didn't incorporate them herewith for the in-depth characterizations of the ACs. In the course of approximating their peak heights (*H*), *FWHMs* (β), and the total area (*A*) underneath them, neither the XRD count intensity (cps) scales were found to be fitted accurately to the standard *Gaussian* convolution nor these variables dependent physicochemical properties were directly derivable. Therefore, no further critical descriptions and premier comparisons among these AC samples can be carried out. However, few additional explanations and quantitative interpretations based on

their XRD patterns, XRD derived observables, and the closely associated variables with that of the both hard and soft type carbon black samples are presented below.

According to the diffractograms measured for the carbon black samples CB1, CB2, CB3, and CB4 shown in Figure 2─Figure 5, the first lower range 2θ angles in which the relatively sharp

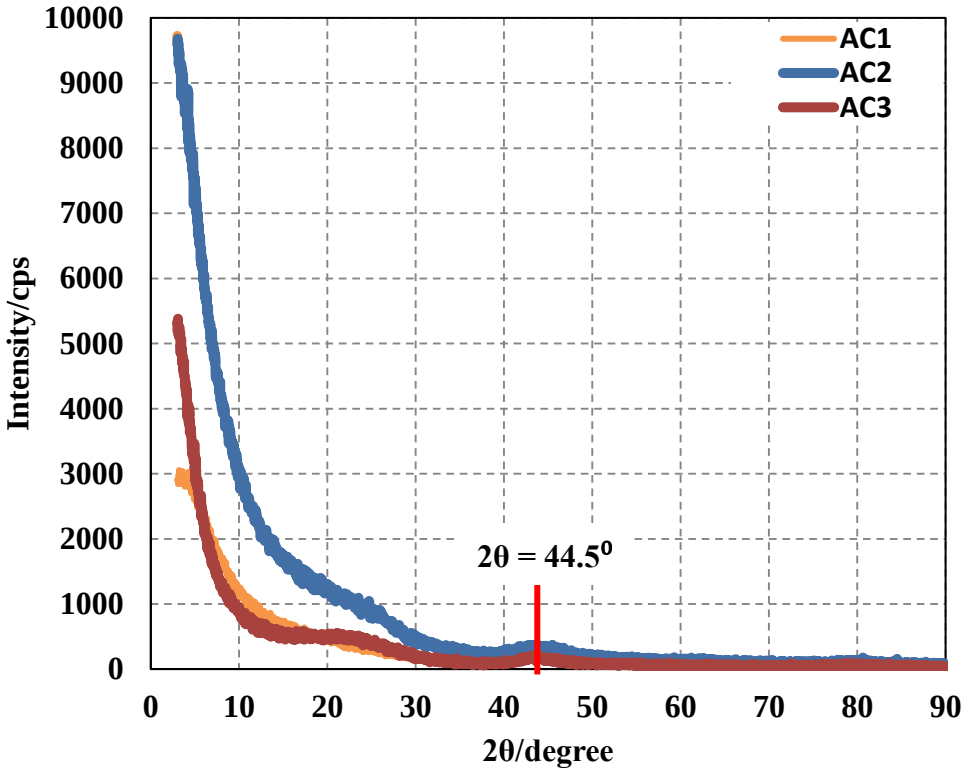

Figure 1. The X-ray diffraction spectra for activated carbon samples AC1, AC2, and AC3 carbonized at ~600─900°C.

XRD spectral bands arose are lying in between 19.5°─26.1° whereas the second higher range 2θ angles in which the broad bands protruded are in between 45.3°─42.8°. If the second angular bar of each of the carbon black samples, and their low XRD counts cum intensity ratio peaks are compared with that of the broad bumps of the activated carbons appeared at the almost identical 2θ angular regime (Figure 1), the latter bands are observed as absolutely negligible as shown in Figure 6; wherein the XRD measured datasets for the typical graphite are plotted for the quantitative comparisons. And, if the similar type quantitative interpretations of the low range 2θ

angular values, and the intensity ratios of the therewith arose spectral bands of both type carbonaceous materials are made, the very predominating peaks with relatively high degrees of acuteness and sharpness are observed only for the carbon black samples. The actual physical meaning underlying with these quantitative comparisons is all the four carbon black samples are relatively less amorphous than the three different activated carbon samples or do exhibit high degree of crystallinity, more ordered internal layouts of the graphene, more periodical arrangement of the graphitic layers, and better applicative morphological and electrochemical properties. Again, if more closely associated yet quite similar comparative interpretations among the variably graphitized carbon black samples (CB1─CB4) are carried out quantitatively, the internal effects of the graphitizing metamorphic temperature towards proceeding the internal rearrangements, restructurings, and reordering of the graphene layouts; decrement of the amorphicity, increment of the crystallinity, squeezing of the interlayer distances (d), changing of the crystallite sizes (L_c) and crystallite growths, and approaching of the materials towards the graphite, etc., can be made more practical and realistic. The responsible descriptors that were derived from the XRD produced spectral information, and became the quantitative means of their precise judgements are summarized in Table 1 and Table 2. If the XRD derived 2θ angular values of the most intense spectral bands of the CB1, CB2, CB3, and CB4 samples are referred (third column of Table 1),

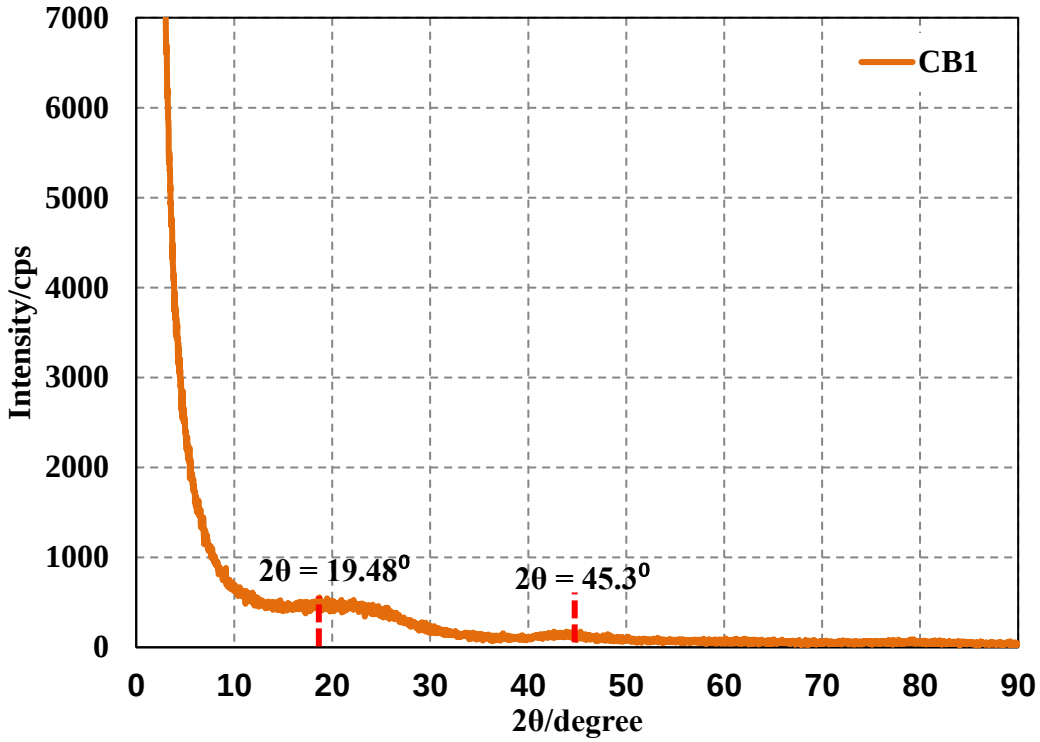

Figure 2. The X-ray diffraction spectrum for carbon clack CB1 carbonized at ~800°C.

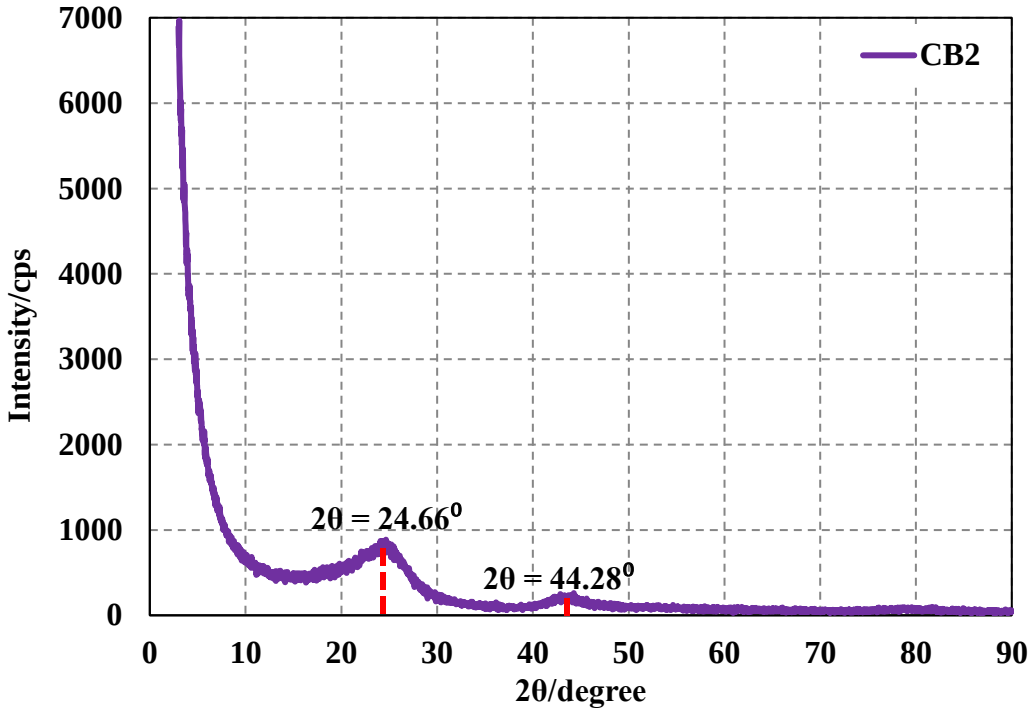

Figure 3. The X-ray diffraction spectrum for carbon clack CB2 graphitized at ~1400°C.

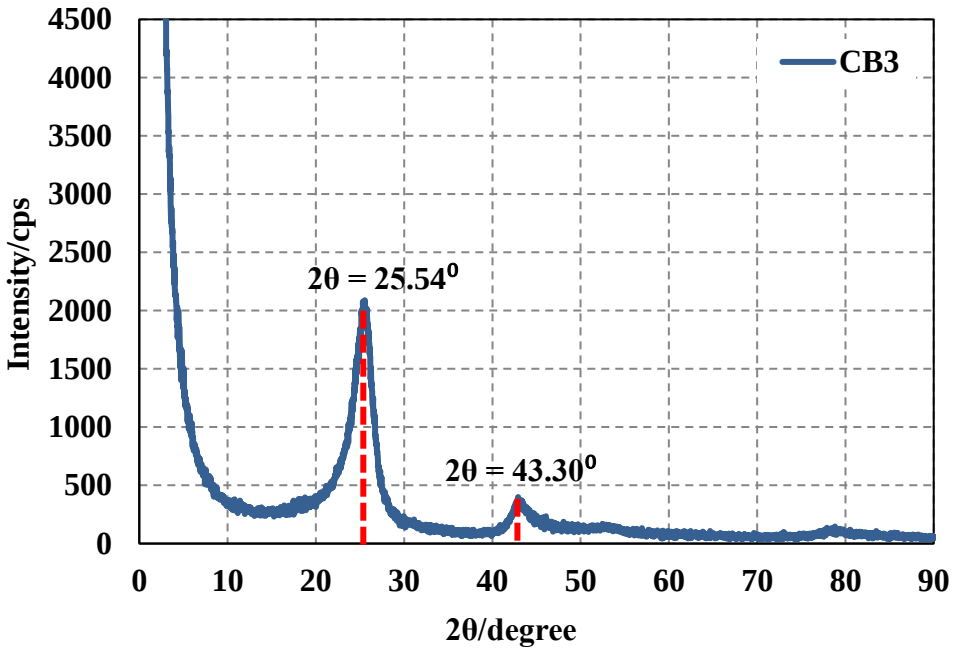

Figure 4. The X-ray diffraction spectrum for carbon clack CB3 graphitized at ~2000°C.

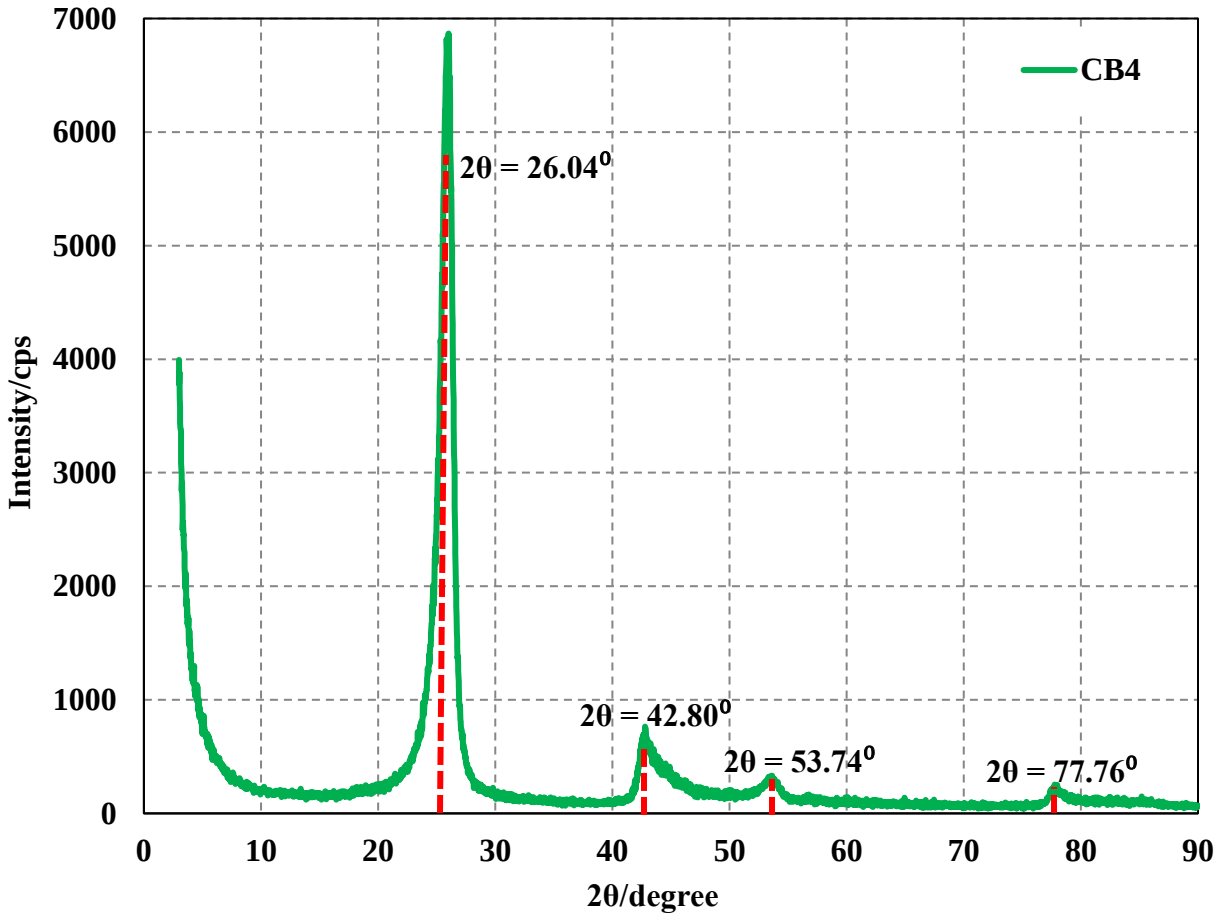

Figure 5. The X-ray diffraction spectrum for carbon clack CB4 graphitized at > 2500°C.

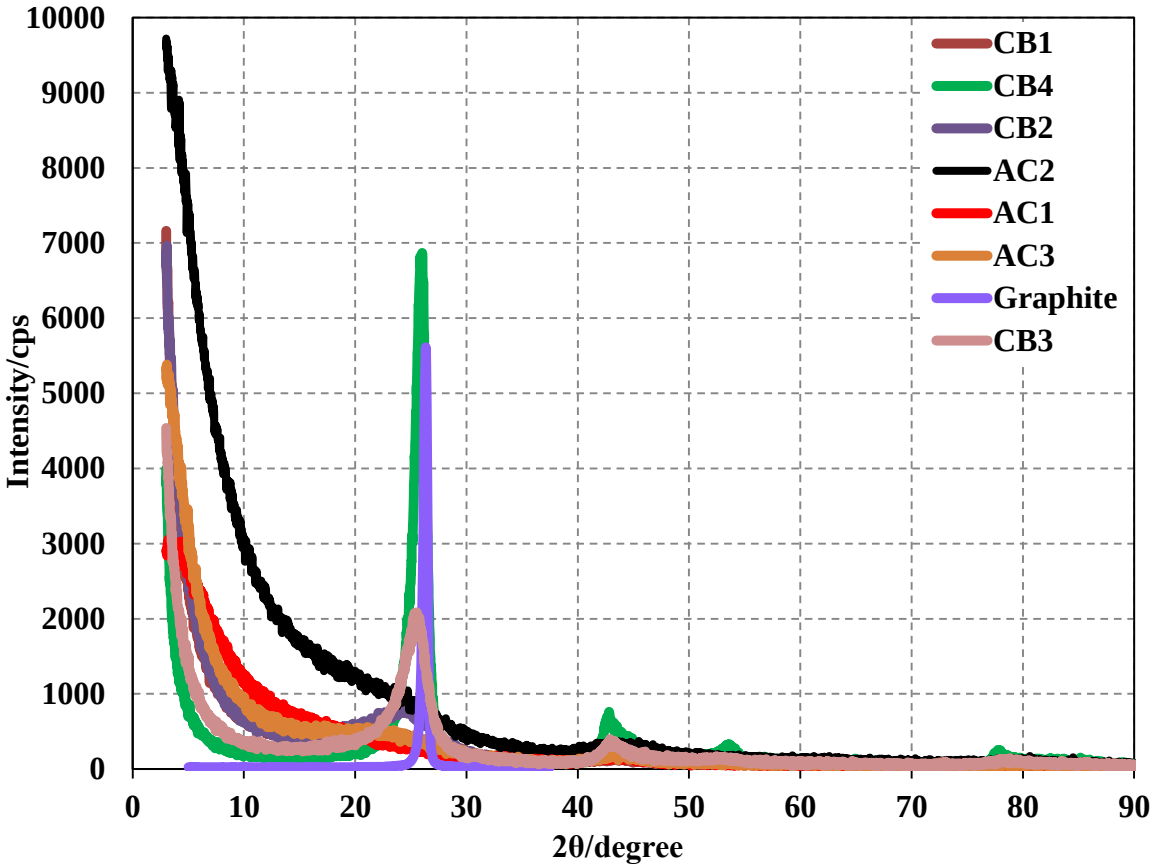

Figure 6. Comparison of the XRD patterns of the carbon materials heated at different temperature regimes. The diffraction datasets for the graphite are also plotted for comparison purpose.

the trend of attaining more and more 2θ angular value towards enriching the typical graphitic band (2θ = 26.4°) is CB1 (2θ = 19.48°) < CB2 (2θ = 24.66°) < CB3 (2θ = 25.54°) < CB4 (2θ = 26.04°). It further means the gap between such a 2θ value of the carbon black samples and that specific to the graphite band follows the order CB4 < CB3 < CB2 < CB1. This angular approaching of the 2θ value towards the typical graphite or semi-graphite further deduces the fact that (a) the degree of amorphicity goes on increasing as CB4<CB3<CB2<CB1, and (b) the degree of crystallinity goes on decreasing as CB4>CB3>CB2>CB1. Accordingly, if the 2θ values assigned to their second most intense yet quite broad bumps are referred; CB1: $2\theta = 45.34^0$; CB2: $2\theta = 44.28^0$; CB3: $2\theta = 43.30^0$; and CB4: $2\theta = 42.80^0$, the same ascending and descending trends of amorphicity and

crystallinity respectively are furthermore justified (this angular regime for the graphite and graphite resembling materials in which the broad XRD bumps are protruded is $2\theta = 41^0$—47^0 [27]). The unique yet low intensity broad bands appeared at $2\theta = 53.74^0$, and $2\theta = 77.76^0$ for the sample CB4 only verify its highest degree of crystallinity or the lowest amorphicity among others (the pure graphite has these values at $2\theta = 54.6^o$ and $2\theta = 77.7^o$ respectively [28, 29]). The major conclusion we extract from all those 2θ angular values diffracted by the internal graphene phases of the four different carbon black samples is the existence of considerable yet dissimilar degrees of crystallinity, ordered layouts of the graphene layers with the optimum restructuring of the C—C networks, and maximum internal rearrangement of the fundamental graphitic units in them. The same is furthermore strengthened by the significant change in interlayer distance (d_{CB}) (Bragg's Law, Eq. 1) calculated for all the four carbon black samples. For the accurate approximation of this, the designated 2θ angular value of the most intense spectral band of each of them were substituted in Eq. 1, and the respective d_{CB} value was determined as summarized in Table 1 (fourth column), wherein the standard literature values *d* computed for those carbonaceous materials that were heated at as equivalent graphitizing temperature as present carbon black samples are listed for the quantitative comparison. Thus calculated values for them are: CB4 = 0.339 nm; CB3 = 0.346 nm; CB2 = 0.358 nm; and CB1 = 0.453 nm, and fortunately, none of them are found to be deviated to those of the literature values [5, 7, 8, 22]. The most important information acquired through these d_{CB} analyses is that the sample CB4 having the lowest (highest) degree of amorphicity (crystallinity) possesses the lowest value of the interlayer distance *d*. It means the sample CB4 has more finely packed graphene layers with the highly squeezed interlayer distance, and hence, it tends to approach more towards the graphite (d = 0.33354 nm) than the others. This closeness goes on decreasing for the rest of the samples as CB3>CB2>CB1. Based on the industrial

Table 1. The Bragg's law derived interlayer distance *d* (basal spacing) of the variably graphitized carbon blacks.

Carbon Samples	Graphitizing Temp. (^{0}C)	XRD-band (^{0})		Interlayer distance *d* (*nm*)	
		2θ	θ	Present work	Lit.[5, 7, 8]
CB4	>2500	26.04	13.02	0.339	0.342
CB3	~2000	25.54	12.77	0.346	0.345
CB2	~1400	24.66	12.33	0.358	0.365
CB1	~800	19.48	9.74	0.453	0.428
AC1, AC2, AC3	~600─900	No sharp X─ ray diffraction bands			

Table 2. The Scherrer's formula derived crystallite sizes L_c, and number of parallel graphitic planes (*m*) of the variably graphitized carbon blacks.

Carbon Samples	Graphitizing Temp. (^{0}C)	*FWHM* (*β*) (*rad.*) (2θ band)	Crystallite size L_c (*nm*)		No. of parallel graphitic planes (*m*)
			Present work	Lit.[6, 7, 8]	
CB4	> 2500	0.0294	5.96	6.6	18
CB3	~2000	0.0363	4.08	3.8	12
CB2	~1400	0.0930	1.59	1.8	5
CB1	~800	0.1483	0.989	1.00	2

graphitizing temperature scales for each of them (Table 1), the CB4 obviously was manufactured with more internal rearrangement or restructuring of the founding graphene layers and graphitic planes than the others, and the same consequences are quantified herewith by its XRD derived magnitude of *d* or by the substantial contractions observed in its basal spacing owing to the existence of highly packed networks of graphitic planes internally. Therefore, in terms of the packing tendencies of the differently aligned graphitic planes, the order among the carbon black samples follows the trend CB4>CB3>CB2>CB1. Accordingly, the closely correlated predominant crystallite size (L_c) that varies significantly upon the variation of graphitizing temperatures, amorphicity/crystallinity, and internal packing coefficients is incorporated herewith as an another potential descriptor in order to identify the internally improvised graphite resembling crystal structure of the carbon black samples. The Scherrer's formula (Eq. 2) derived L_c value for each of them is summarized in Table 2 (fourth column) wherein the most relevant literature values are cited. The *FWHM* (*β*) value required for determining the concerned L_c was computed by the *Gaussian* peak fitting technique. The Figure 7─Figure 10 verify the extent to which the entire

datasets between the *Gaussian* convolution and the most intense XRD protrusion of every individual carbon blacks are fitted. The insets of them are listed with all those β values. The L_c value for each individual carbon black sample is; CB4: L_c = 5.96 nm, CB3: L_c = 4.08 nm, CB2: L_c = 1.59 nm, and CB1: L_c = 0.989 nm; suggesting that the carbon black materials that tend to resemble more to the graphite gains relatively bigger crystallite size or growth. This is also in accordance with the temperature dependent characteristic features of the materials and their crystal growth propensities: when the graphitizing temperature goes on increasing, the more and more internal orderings of the graphitic planes take place, and the better is the crystallite growth and sizes (L_c) leading to the entire development of the ultrafine carbon crystals possessing recognizable Lattice parameters and Bravais Lattices in the three dimensional space and considerably lower crystallographic defects [30]. Therefore, the internal crystal growth rate and the attainment of the graphite crystal like geometrical shapes goes on decreasing as: CB4>CB3>CB2>CB1. Moreover, another quantitative descriptor that explains the occurrence of the crystal growth or the extent to which an internal improvisation of the graphene orderings takes place upon the heat treatment procedures is XRD derived *m* value (the numeral value that can approximate the actual number of the parallel graphene layers interlocked each other by the weak Van der Waals forces). The calculated value of it for each individual carbon black sample (Eq. 4) is summarized in Table 2 (fifth column); CB4: *m* = 18, CB3: *m* = 12, CB2: *m* = 5, and CB1: *m* = 2; ensuring that the carbon sample having the better growth of the crystallites (L_c) exhibits better ordered and higher numbered graphene layers. This is well agreeable observation as the highly graphitized carbonaceous materials always lead to the massive internal restructuring and reprocessing of the graphene layers, and the resulting matrix often contains more periodic and homogeneous graphene orderings.

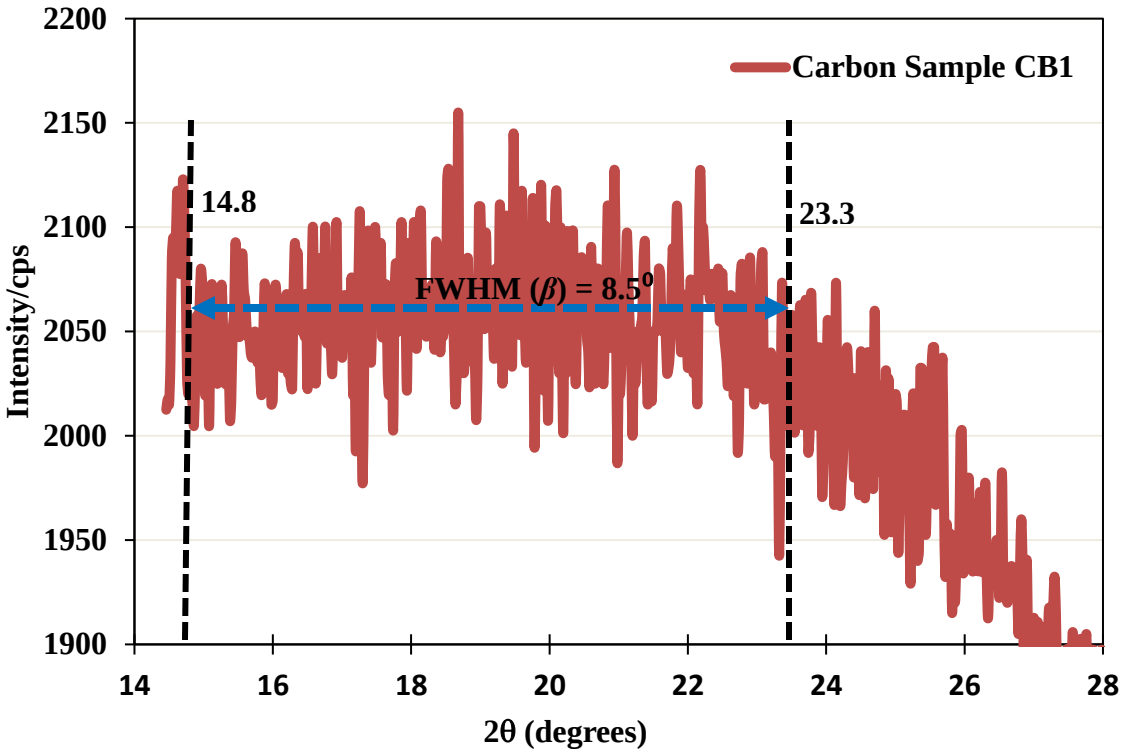

Figure 7. The diffusive XRD peak of carbon sample CB1 protruded at 2θ = 19.48°. The manually calculated *FWHM* value is mentioned in the inset (the *Gaussian* convolution peak fitting technique was impracticable due to extreme peak-broadening and obtuseness).

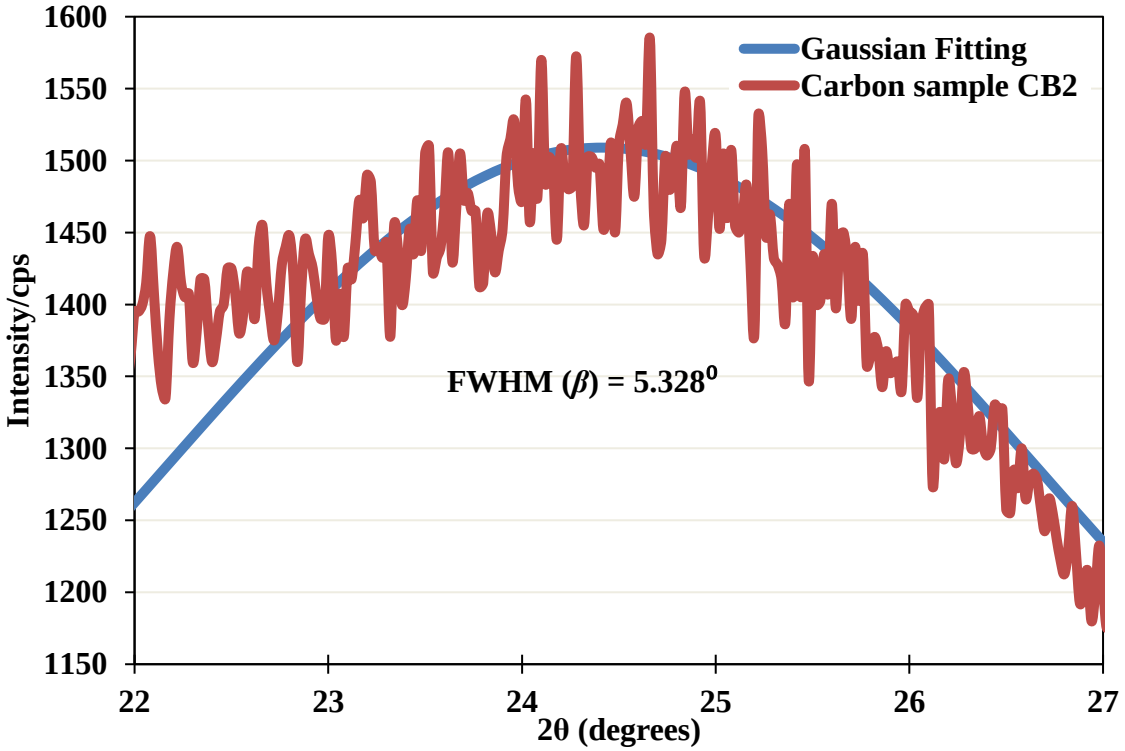

Figure 8. The broad yet relatively intense XRD peak of carbon sample CB2 appeared at 2θ = 24.66°. The *FWHM* value is mentioned in the inset.

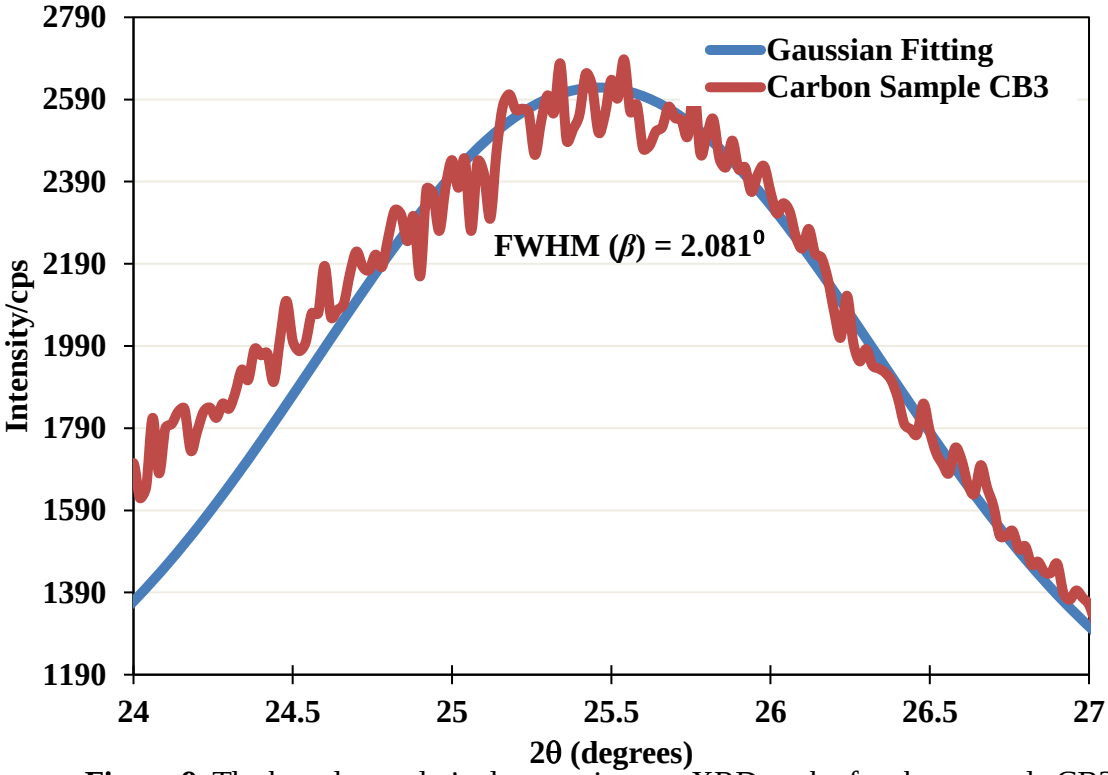

Figure 9. The broad yet relatively more intense XRD peak of carbon sample CB3 appeared at 2θ = 25.54°. The *FWHM* value is mentioned in the inset.

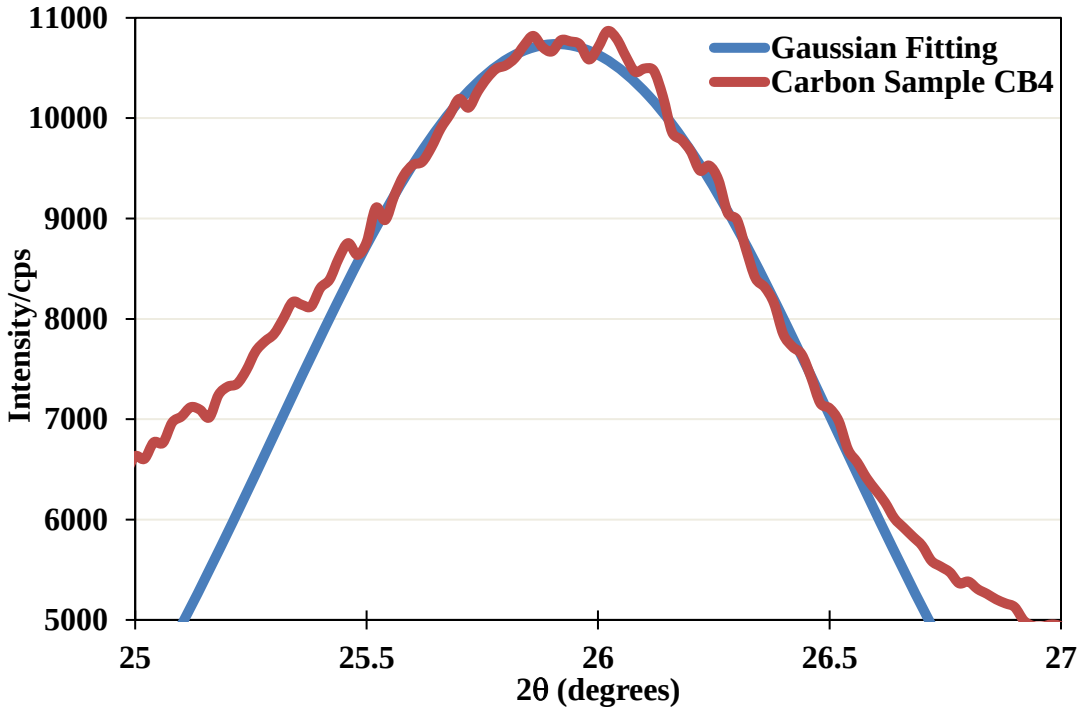

Figure 10. The relatively most intense XRD peak of carbon sample CB4 appeared at 2θ = 26.04°. The *FWHM* value is mentioned in the inset.

Based on the above mentioned XRD derived descriptors including 2θs, intense and broad spectral bands, interlayer distance d_{CB}, crystallites sizes (L_c) and growth, and number of parallel graphene planes (m), the low carbonization temperature manufactured and lower graphitizing temperature treated carbonaceous materials are found to gain the least improvised characteristic features such as higher (lower) amorphicity (crystallinity), lower graphene orderings, lower contraction in the basal spacing, lower crystal growth and crystallite sizes, higher sporadicity of the graphene layouts, more intertwined C─C networks, etc. But, the same features actually mark themselves as the most potential carbon materials towards utilizing industrially for designing faithful carbomasks, face paints, ultrafiltration technologies, and professional cosmetic products [31] besides bestowing electrode and electroactive materials, masks technology, electrocatalysts and photovoltaic cell technology, etc. type promising attributes. If the present XRD predicted crystallite sizes (L_c) and crystal growth propensities, agglomeration tendencies of the crystallite particulates into the grains cum particles, etc., are referred, the activated carbons AC1, AC2, AC3, and the first two carbon blacks CB1 and CB2 are speculated as more preferable materials towards the development of professional grade commercial products such as (a) cosmetics: eyeliner, mascara, nail polish, eye shadow, lipstick, brushers, make up, foundations, rouge, etc.; (b) face paints with no pores-clogging, anti-irritations, scrubbing free, and easily washable and wipeable features; (c) filtration solutions: wastewater, foul gaseous, feedstock impurities and contaminants, filter bags, multi ply face masks; (d) sunscreens; (e) wound healing and high drug-loading products; etc. [32]. But, the relatively more advanced potentialities and applicative domains gained by the highly graphitized carbonaceous materials such as CB3 and CB4 are predicted in the subsection 3.2 wherein the same XRD estimated parameter sets are taken into account for further justifications.

3.3 XRD Correlated Metamorphic Changes

Alike to the determination of the *FWHM* (β) values of each carbon black sample through the *Gaussian* peak fitting procedures, the effective net area (A) lying under the designated XRD spectral bands was estimated using the standard relation formulated in Eq. 5. This area (mm^2) (Table 3, second column) approximated for every carbon samples was substituted in Eq. 6 for determining their percentage crystallinity (%C). Since the degree of crystallinity always conveys the extent to which the graphene layers undergo internal orderings/restructurings or the heterogeneous layouts of the basic structural units turn into the more or less homogeneous arrangement, it's precise magnitudes for differently graphitized carbonaceous materials (Table 2, fourth column) act as the central means of speculating their microstructural layouts of the founding crystallite phases. The higher %C always signifies the existence of wider dissimilarity between the specific carbon material and the graphite in terms of their internal homogeneity of the graphitic planes and their orderings [8]. That is, the carbon materials having a higher %C always need more rigorous physicochemical conditions (controlled heating, annealing, calcinations, oxidative heat and chemical treatments, catalytic graphitization using minerals and metals as catalysts, etc.) for converting their sporadically arranged graphitic layouts into the homogeneous patterns. The lowest %C estimated herewith for the CB4 sample (%C = 1.3%) illuminates that its' internal graphene layouts are more like graphite; *i.e.* this particular carbon black sample resembles quite well to the graphite internally, and hence, can be converted into the latter *via* more convenient yet least aggressive modifications and conversions techniques. But, the sample CB1 with the highest calculated value of %C = 19.63% signifies its quite contrasting yet incomparable internal heterogeneity to that of the graphite and semi-graphite (such as CB4), but still offers some possibility of restructuring their founding crystallite phases with relatively more diligent and stern

conversion criteria. If the calculated value of the %*C* elsewhere [8] for the pet coke material (%*C* = 12.6%) is referred, it can be depicted that the pet coke could be graphitized and transformed into the graphite resembling material relatively easier (harder) than the CB1 (CB4, CB3, CB2). Therefore, in reference to the farness of the internal founding graphene layouts to that of the graphite, and the complex conversion requirements needed for restructuring/reconfiguring themselves into the graphite like graphene moieties, the four carbon blacks can be arranged as CB4 < CB3 < CB2 < CB1. This observation itself is also supporting why the degree of amorphicity is lowered, internal orderings of the graphene layouts become better, and the structural heterogeneity is subsequently improved upon the increment of the graphitizing metamorphic temperature regimes succeedingly. In a similar manner, the extent of the graphitization orders or the degree of graphitization (% DOG) (Table 3 (third column)) speculated for all the four carbon black samples are helpful to measure the exact quantity of the internally arranged sproradical graphene layouts restructured into the graphite like systematic patterns upon the progressive graphitizations of the carbonaceous materials. The %DOG also approximates how closely the carbonaceous materials are approaching towards the typical graphite by reconfiguring their internally arranged graphitic domains. The computed values of it (Eq. 7) for the present four carbon black samples are: CB4 = 98.36 %; CB3 = 96.26 %; CB2 = 92.67 %; and CB1= 64.48 %. This trend of lowering the % DOG by lowering the graphitizing temperature scales ensures us that the substantial reshuffling of the internal graphitic domains takes place, and the tendency of undergoing the same is extremely sensitive to the internally acquired metamorphic temperature regimes. Since the sample CB4 attained the highest graphitizing temperature (>2500^{o}C) scale for reshuffling its internal positioning of the graphene layers during its manufacturing stages, the 98% *DOG* of it simply exemplifies that only around 2% of its internal graphene layouts is dissimilar to that of the graphite.

In this sense, among the four carbon black samples, the CB1 holds the maximum (minimum) extent of the amorphicity (crystallinity) having only ~ 64 % internal graphene layouts similar to the graphite. If the literature [8] %*DOG* value calculated for the pet coke material is referred, it is found as 95%, and that for the semi-graphite and graphite approaching materials are 70%─81%, and 82%─98% [17] respectively; justifying the accuracy range of the present XRD measurements and the relevant %*DOG* estimations. Since the % *DOG* is found to be very much correlated to the internal heterogeneity or the extent to which the core granular structures of the non-graphitic carbonaceous materials are differed to that of the crystalline graphite [17], the descriptors ρ and u furthermore elucidate the real magnitudes of the structural disorders and the associates quantitatively. The explicit calculated values (Eq. 9a, 9b) of them for each of the carbon black samples are listed in Table 4 (fifth and sixth columns). The lower magnitudes of the former signify the lower (higher) degree of the internal graphitic disorders (orders), and those that are scaled as >1 indicate the existence of incomparable deviations in the interlayer distance d to that of the fully ordered graphite (d = 0.33354 nm).

The next important descriptor is a metamorphic temperature ($T_{met.}$) that actually quantifies the frequency of increasing internal kinetic energy gradually upon the increment of the graphitizing temperature scales, and measures the exact effects of the latter towards the internal shifting of the core atomic positions (vibration of the atoms) of the graphene layers within the definite crystal lattice consecutively. The specific values of it for the individual carbon black samples CB4, CB3, CB2, and CB1 calculated on the basis of %*DOG* are summarized in Table 3 (fifth column): $T_{met.}$ = ~595°C, ~588°C, ~577°C, and ~486°C respectively. Practically, the metamorphism means the increase in internal kinetic energy due to increase in motion of the basic structural domains/atoms /molecules of the materials induced by the externally supplied heat sources, internal pressure

confinements, and many other directed granular stresses/strains so as to change their core compositions and/or surficial textures without disrupting the crystalline frameworks. The first inducing factor causes vigorous atomic swapping, and the second leads to surpass any types of the internal stresses and strains responsible for altering the ideal shapes and sizes of the crystallites and their growth rates, textures plus functionalities of the particulates cum grains, and many other recognizable metamorphisms [34]. Based on these metamorphic effects occurring into the granular cores of the materials, and the closely associated graphitizing temperature regimes of the presently sampled four carbon blacks, the maximum internal kinetic energy gained by their atomic constituents follow the order; CB4>CB3>CB2>CB1. It means the optimum metamorphic changes including internal reordering, restructurings, reconfiguring, reshuffling, and swapping of the C atoms of the basic graphitic domains, and thereafter proceeded predominant improvisations in the crystallite sizes, shapes, and 3D crystallite growth, etc. are acquired by the CB4 sample followed by the CB3, CB2, and CB1. According to the literatures [17, 34], the critical metamorphic temperature scale above which the pronounced packing of the graphene layers or the substantial reduction in their basal spacing (*d* values) occurs gradually is 400°C, and it is ≤ 300°C for the semi-graphite type materials. And, the graphite approaching carbonaceous materials whose *DOG* are computed as ~ 96% and ~ 64% are found to gain T_{met} = ~588°C and ~ 492°C respectively plus the reduction in the magnitude of the *d* value when the T_{met} is increased by 24°C is almost 0.0001nm [17]. These analogies are also found to lie in a very agreeable range to the presently computed datasets of the %DOG and T_{met} (Table 3). Nevertheless, all those internal effects of the T_{met} in terms of enlarging (reducing) % crystallinity (amorphicity), % *DOG*, crystallite growth size L_c, and of contracting the basal spacing, etc., of the present four carbon black samples are well justifiable to the premier results and discussions presented in aforementioned paragraphs.

Table 3. The calculated values of graphitization degrees (%) and crystallinity (%) of the variably graphitized carbon blacks.

Carbon Samples	Area under 2θ band (mm^2)	Degree of Graphitization (DOG) (%)	Crystallinity (C) (%)	Metamorphic Temp. (T_{met}) (°C)
CB4	14918.245	98.36301	1.323	594.76
CB3	3730.1829	96.26432	5.088	588.03
CB2	3239.9303	92.66654	5.814	576.53
CB1	816.07399	64.48402	19.683	486.34

Table 4. The calculated values of X-ray density (ρ_{XRD}), BET surface area (S_{BET}), and specific capacitance (C_{SP}) of the variably graphitized carbon blacks.

Carbon Samples	X-ray density (ρ_{XRD}) (g/cm^3)	BET surface area ($S_{BET} \approx S_{XRD}$ (m^2/g)	Specific capacitance C_{SP} (F/g)	Structural disorder (ρ)	Degree of structural order (u)
CB4	2.2295	5348.11	600.06	0.633	0.367
CB3	2.1867	3735.38	419.11	1.083	0.083
CB2	2.1113	1508.44	169.25	1.614	0.614
CB1	1.6678	1186.45	133.12	3.697	2.697

In material characterizations, the quantitative analyses of the surface area; the most critical morphological observable attributing to the designs and manufactures of the solid states and porous type materials, are performed by means of the BET adsorption principles [35]. It enables us to reveal the physical structure, degree of the porosity and porous interior/exterior walls, heterogeneous surface morphologies and the extent of the internal heterogeneity, etc., type in-built characters and functionalities of the materials. In particular to the carbonaceous materials, predicting somewhat accurate magnitudes of the BET surface area (S_{BET} (m^2/g)) is very much essential to understand many other indispensable industrial applicative properties such as dissolution rates, catalytic performances, moisture retention, ultrafiltration and microfiltration propensities, internal packing coefficients, core granular compositions, etc. The activated carbon for example exhibits less or more than 2000 m^2/g specific surface area (BET area) (it is subjected to change considerably upon changing the carbonization/graphitizing temperature scales), deducing the presence of high degree of porosity and porous networks in it because of which

massive functionalisations are implemented industrially [35─37]. The BET surface areas S_{BET} (m^2/g) determined in this study (Eq. 10) for the variably graphitized and differently metamorphosed carbon black samples are summarized in Table 4 (third column). The S_{BET} value for them are; CB4 = 5348 m^2/g, CB3 = 3735 m^2/g, CB2 = 1508 m^2/g, and CB1 = 1186 m^2/g. It depicts that the first sample bears the highest degree of roughness, heterogeneous surface textures, and porous & porosity networks within its particulates cum grains interiors & exteriors followed by the latter samples consecutively. In reference to the S_{BET} dependent industrial applicative domains such as reinforcing strength to the rubber; pharmaceutical ingredients, binders, and lubricants; heterogeneous surface catalysts and electro-catalysts; anodes, cathodes, and separators type electroactive spare parts; semiconductor and microchips designs; etc., the working performances of these carbon blacks follow the order: CB4>CB3>CB2>CB1. More particularly, this descending order vows to forecast their many other functionalizable physicochemical properties such as decrement in (a) wear and tear resistance, (b) dissolution and cohesion, (c) reaction kinetics and products yields, (d) catalytic potentialities, (e) charging/discharging cycles, (f) impedance lowering, and (g) ions/molecules/charge/energy- storing capacities; etc. [35]. The calculated S_{BET} values reported elsewhere [9, 36, 37] for the carbonaceous materials graphitized/ carbonized in between 600°C─1000°C are in the range of 3400 m^2/g─4400 m^2/g, and those categorized under low and very low structured carbon blacks are ~600 m^2/g─2100 m^2/g; the quite consistent experimental values to those determined in this study if the internal effects of the calculated metamorphic temperature scales of the present four carbon black samples are practically considered. Accordingly, the electrochemical descriptor that has a strong mathematical linkage with the S_{BET} (m^2/g), and can quantify the net amount of the charge stored per unit mass of the carbon materials while employing the same as potential electrode materials for the batteries,

capacitors, supercapacitors, sensors, etc. is a specific capacitance C_{SP} (F/g) (Eq. 12). The concerned values of it estimated herewith for the variably carbonized/graphitized carbon black samples (CB4 (C_{SP} = 600 F/g), CB3 (C_{SP} = 419 F/g), CB2 (C_{SP} = 169 F/g), and CB1 (C_{SP} = 133 F/g)) are listed in Table 4 (fourth column). If they are compared in reference to the metamorphic effects of the graphitizing temperatures in changing %*DOG*, %*C*, L_c, *d*, amorphicity, S_{BET}, etc. of the CB1─CB4 carbon black samples, the greatly improvised CB4 is found to exhibit the highest capability of storing maximum amount of the charge per unit mass of it followed by the others serially. This comparison furthermore depicts that the CB4 must be enriched with the optimal pore structures having diverse porosities ranging from macro to micro porous pores in its interior walls /surfaces of the founding particulates followed by the others. According to the literatures [23, 38], the nitrogen doped porous carbons prepared through the facile carbonization (700°C)/activation strategy offers the S_{BET} 2248 m^2/g and the C_{SP} 341 F/g [38], and that for the activated carbon monoliths porous electrodes characterized with only the micro- and meso- porous pores are S_{BET} = 1656 m^2/g, and C_{SP} = 141 F/g [23]; justifying the consistency regimes of the presently determined S_{BET} and C_{SP} values specific to the dissimilarly graphitized carbon black samples. Present author has practically utilized each of these carbon black samples for making anodic and cathodic materials of the vanadium redox flow battery cell, and studied their working performances in terms of oxidizing/reducing propensities to the V(II)/V(V) electrolyte ions, electrochemical reaction kinetics and cell reaction-products yields, charging/discharging stabilities, impedance lowering attributes, ions/molecules/charge/energy storing capacities, and electrocatalytic potentialities. The detailed analyses are yet to be carried out.

4. CONCLUSIONS

This research work was primarily aimed at characterizing the variably metamorphosed and graphitized carbonaceous materials (activated carbons (AC1, AC, AC3): T = 700°C─900°C; and carbon blacks (CB1, CB2, CB3, CB4): T = 800°C─ >2500°C) manufactured from the wide-range carbon precursors carbonized under complete absence of oxygen industrially. These carbon materials were priory claimed as potential applicative material domains, and were expected to possess promising morphological, thermal, mechanical, electrochemical, electrical, and electronic properties with high (a) degree of porosity/porous networks and heterogeneous textures, (b) specific surface area, (c) irregularity in the pores shapes and sizes, (d) electrical-energy-storing and conductive propensities, (e) thermal expansion resisting and chemical stability retaining features, etc. However, the most critical effects of the variable range graphitizing and metamorphosing temperature regimes in transforming their internal degrees of amorphicity and crystallinity, crystallite sizes and growths, sporadical graphene layouts and graphitic domains, graphene layer packing ratio, etc., and the closely associated consequences underlying into all those functional physicochemical properties were not studied. Herewith, few selected mathematical descriptors (intensities (I), area (A), and 2θ angles of the XRD bands, intergraphene layer distance (d), crystallite size (L_c), number of the parallel graphene layers (m), degree of graphitization ($\%DOG$) and crystallinity ($\%C$), metamorphic temperature (T_{met}), degree of structural disorder (ρ) and order (u), BET adsorption surface area (S_{BET}), and specific capacitance (C_{SP})) that have closed linkages to the concerned X-ray diffraction patterns of the every carbon samples were employed explicitly, and the in-depth metamorphic changes and internal modifications were sought out. Besides these, the exact quantifying aptitudes and significances of

each of these descriptors in speculating various functional properties of such a dissimilarly carbonized and graphitized carbon materials were theorized.

The closed analyses of the broad yet diffused XRD protrusions bumped at 2θ = 44.5° exemplified the absolute presence (absence) of the high degree of amorphicity (crystallinity) in all the three AC samples whereas somewhat negligible bumping about to appear at $2\theta = 25^0$—27^0 elucidated their gradual structural transforming abilities into the progressive crystalline materials (applicative domain) upon improvising their graphitizing scales. However, the pronouncedly intensive and broadly diffusive bands arose respectively at 2θ = 19.5°—26.1° and $2\theta = 45.3^0$ — 42.8^0 of the CB samples justified their higher (lower) degree of crystallinity (amorphicity) with more ordered and periodical graphene layouts than that present in the ACs. In terms of the magnitudes of the diffraction angle (2θ) approaching more towards the graphitic values (2θ = 26.4^0, 41^0—47^0, 54.6°, and 77.7°), the CBs were found to follow the order: CB4 ($2\theta = 26.04^0$, 42.80^0, 53.74^0, 77.76^0) > CB3 ($2\theta = 25.54^0$, 43.30^0) > CB2 ($2\theta = 24.66^0$, 44.28^0) > CB1 (2θ = 19.48°, 45.34^0). The Bragg's law derived intergraphene layer distance d (CB4 = 0.339 nm; CB3 = 0.346 nm; CB2 = 0.358 nm; and CB1 = 0.453 nm) furthermore ensured this trend of resembling graphite (d = 0.33354 nm) along with justifying the gradual contractions occurred in their crystallites upon graphitizing themselves. This temperature dependent crystallite characters were also guaranteed by the Scherrer's formula produced L_c value: CB4 = 5.96 nm, CB3 = 4.08 nm, CB2 = 1.59 nm, and CB1 = 0.989 nm, quantifying the occurrence of successive growths of the crystallites progressively. Accordingly, the %C calculated for each of these CB samples was found to be well agreeable in reference to the extent to which more or less rigorous criteria are required to transform their internal graphene layouts closer to the graphite: the CB4 (%C = 1.3%) and CB1 (%C = 19.63%) were recognized as contrastingly different carbon matrices as the former needs

less aggressive modifications and conversions techniques than the latter. The % *DOG* determined for them actually measured the quantitative amounts of their restructured graphene layouts: CB4 = 98.36 %, CB3 = 96.26 %, CB2 = 92.67 %, and CB1 = 64.48 %, and verified the descending trend of reshuffling graphene layers upon the decrement of the graphitizing temperatures. The % *DOG* dependent ρ and u descriptors were furthermore applied to judge their internal degrees of heterogeneity, and found to possess dissimilar graphitic orderings in a core-level. The T_{met} was computed to analyze their internal metamorphic changes including reordering, restructuring, reconfiguring, reshuffling, and swapping of the C atoms of their basic graphitic domains, and thereafter proceeded predominant crystallite growths and sizes, and the resulting trend was observed as CB4 (~595°C) > CB3 (~588°C) > CB2 (~577°C) > CB1 (~486°C). The exact change in surface morphology, roughness, heterogeneity, and porous & porosity networks in their particulates interiors and exteriors upon changing the T_{met} were evaluated through the calculated magnitudes of the S_{BET} (m^2/g), and again found to hold the same continuity: CB4 (5348 m^2/g) > CB3 (3735 m^2/g) > CB2 (1508 m^2/g) > CB1 (1186 m^2/g). Additionally, the capability of storing maximum amount of the charge per unit mass of them while employing as electrode materials separately was studied by means of the calculated magnitudes of the C_{SP} (F/g): CB4 (600 F/g), CB3 (419 F/g), CB2 (169 F/g), and CB1 (133 F/g), and was observed to embrace the same graphitization ideologies. These downward trends of the S_{BET} and C_{SP} indicators accordingly forecasted their applicative functionalities such as compressibility and reinforcement, binding and lubrications, heterogeneous catalysts and catalysis, electroactive anodes, cathodes and separators, semiconductors and microchips accessories, etc., and illuminated their grainy matrices full of wide range pores and porosity networks. The series of the sophisticated experimental investigations are recommended to materialize thus speculated functional properties genuinely.

ACKNOWLEDGEMENT

This research project was fully funded by Brother Industries, Ltd., Japan. The Institute for Material Research (IMR), Tohoku University, Japan is acknowledged for granting this project. The author is thankful to the entire editorial and reviewer boards for their constructive criticisms.

DECLARATION OF AI USAGE

Author has declared that no any AI tools and the texts generated by them are used.

COMPETING INTERESTS

Author has declared that no competing interests exist.

REFERENCES

1. R.J. Martín-Palma, J. M. Martínez-Duart, Novel Advanced Nanomaterials and Devices for Nanoelectronics and Photonics (Nanotechnology for Microelectronics and Photonics, 2017).
2. R.M. Koenig, H. R. Tian, T.L. Seeler, K.R. Tepper, H. M. Franklin, Z. C. Chen, S.Y. Xie, *Am. Chem. Soc.*,142(36),15614(2020).
3. R. Lian, J. Feng, X. Chen, D. Wang, D. Kan, G. Chen, Y. Wei, A*CS Appl. Mater. Interfaces*, 12(1), 619(2020).
4. T. Takamura, *Carbon Ency. Elect. Power Sources*, 709(2009).
5. T. Denaro, V. Baglio, M. Girolamo, V. Antonucci, A. S. Arico, F. Matteucci, R. Ornelas, *Appl. Electrochem.*, 39, 2173(2009).
6. T. Unga´ra, J. Gubiczaa, G. Riba´rika, C. Panteab, T. W. Zerda, *Carbon*, 40, 929(2002).
7. Z. Liu, J. Wang, C. Li, C. Zheng, B. Zhang, *Materials*, 14(22), 7085(2021).

8. N. Isa, Dissertation: X-Ray Amorphous Pattern Characterization of PETRONAS Petroleum Coke Product as a Potential for Advanced Carbon-Carbon Composite Material Precursors. Universiti Teknologi PETRONAS (2012).
9. M Deraman, N. E. S. Sazali, M. F. Y. M. Hanappi, N. S. M. Tajuddin, E. Hamdan, M. Suleman, M. A. R. Othman, R. Omar, M. A. Hashim, N. H. Basri, N. S. M. Nor, B. N. M. Dolah, A. M. Noor, M. R. M. Jasni, *Journal of Physics*: *Conference Series*, 739, 012085 (2016).
10. H. Liu , W. Zeng, Y.Yang, J. Chen , Y. Zhao, S. Mu. *J. Mater. Chem. A*, 9, 1260(2021).
11. Carbolite Gero GmbH & Co. KG, Graphitisation at up to 3000 °C, Hesselbachstr, 15, 75242, Neuhausen, Germany (2017). Available: *https://www.azom.com/article.aspx?ArticleID=14321*
12. Md S. Reza, S. Afroze, *et al.*, *Sustainability*, 15(8815), 1(2023).
13. J. Gorss, The full history of carbon fibers has yet to be written: the industry is barely out of its infancy, *Americal chemical society*, 2003. Available: *chrome-extension://efaidnbmnnnibpcajpcglclefindmkaj/https://www.acs.org/content/dam/acsorg/education/whatischemistry/landmarks/carbonfibers/high-performance-carbon-fibers-commemorative-booklet.pdf*
14. O. Beyssac, D. Rumble, *ELEMENTS*, 10, 415(2014).
15. J. M. Wrogemann, O. Fromm, F. Deckwirth, K. Beltrop, A. Heckmann, M. Winter, T. Placke, *Batteries & Supercaps*., 5, e202200045, 1(2022).
16. J. Li, D. Yin, Y. Qin, *Manufacturing Rev.*, 10(13), 1(2023).
17. A. Vlahov, G*eologica Balcanica*, 50 (1), 11(2021).

18. J. B. Donnet. Carbon Black: Science and Technology (CRC Press, Marcel Dekker, Inc. New York Basel, 1993).
19. J. I. Langford, J. C. Wilson, *J. Appl. Cryst.*, 11, 102(197).
20. S. N. Ghosh, S. K. Handoo, *Cement and Concrete Research*, 10, 771(1980).
21. H. Wada, T. Tomita, K. Matsuura, *et al.*, *Contr. Mineral. Petrol.*, 118, 217(1994).
22. J. Y. Howe, C. J. Rawn, L. E. Jones, H. Ow, *Powder Diffraction*, 18(2), 150(2003).
23. N. H. Basri, M. Deraman, R. Daik, M. T. M. Ayob, M. I. Sahri, N. S. M. Nor, B. N. M. Dolah, S. Soltaninejad, *Ad. Mat. Res.*, 1112, 236(2015).
24. G. Baral, A. B. Marahatta. *Asian J. Appl. Chem. Res*., 14(4), 34(2023).
25. A. B. Marahatta, P. K. Dhal, *Int. J. Prog. Sci. Tech*., 46(2), 83(2024).
26. Z. Xie, W. Guan, F. Ji, Z. Song, Y. Zhao. *J. Chem.*, 491912, 1(2024).
27. K. R. Hallam, J. E. Darnbrough, C. Paraskevoulakos, P. J. Heard, T. J. Marrow, P. E. J. Flewitt, *Carbon Trends*, 4(100071), 1(2021).
28. S. Müllner, T. Held, T. Tichter, P. Rank, D. Leykam, W. Jiang, T. Lunkenbein, T. Gerdes, C. Roth, *J. Elect. Soc*., 170, 070523, 1(2023).
29. Q. Tul Ain, S. Hyder Haq, A. Alshammari, M. Abdullah Al-Mutlaq, M. Naeem Anjum, *Beilstein J. Nanotechnol*, 10, 901(2019).
30. D. Gonza´lez, M. A. Montes-Mora´n, I. Sua´rez-Ruiz, A. B. Garcia, *Energy & Fuels*, 18, 365(2004).
31. A. D. Colletta, M. Pelin, S. Sosa, L. Fusco, M. Prato, A. Tubaro, *Carbon*, 196, 683(2022).
32. I. Budiman, R. Amirta, Y. Taming, B.A. Widyaningrum, W. Fatriasari, Activated Carbon for Cosmetics Applications. Biomass-based Cosmetics (Springer, Singapore, 2024).
33. M. Bilal, H. M. N. Iqbal, *Cosmetics*, 7, 24(2020).

34. H. Wada, T. Kazuhiro, K. Matsuura, K. Iuchi, M. Ito, T. Morikiyo. *Contrib. Mineral Petrol* 118, 217(1994).

35. Lowell, S. *et al.* Characterization of Porous Solids and Powders: Surface Area, Pore Size and Density. 1st *ed*. (Dordrecht, Springer, Netherlands, 2004).

36. M. Kaya, Ö. Şahin, C. Saka, *Int. J. Chem. Reac. Eng.*, 20170060, 1(2017).

37. A. Kyrlidis, R. M. Sawka, G. D. Moeser, P. A. Kossyrev, N. J. Hardman, High surface area and low structure carbon blacks for energy storage applications, US8895142B2, United States Patent. Available: *https://patents.google.com/patent/US8895142B2/en*

38. J. Yu, N. Fu, J. Zhao, R. Liu, F. Li, Y. Du, Z. Yang, *ACS Omega*, 4(14), 15904(2019).